Research Article

Investigating Synergy of CO_2 and Low Saline Water for CO_2 Storage and Enhanced Oil Recovery

Krishna Raghav Chaturvedi[†], Durgesh Ravilla[†], Waquar Kaleem[†], Prashant Jadhawar[#],
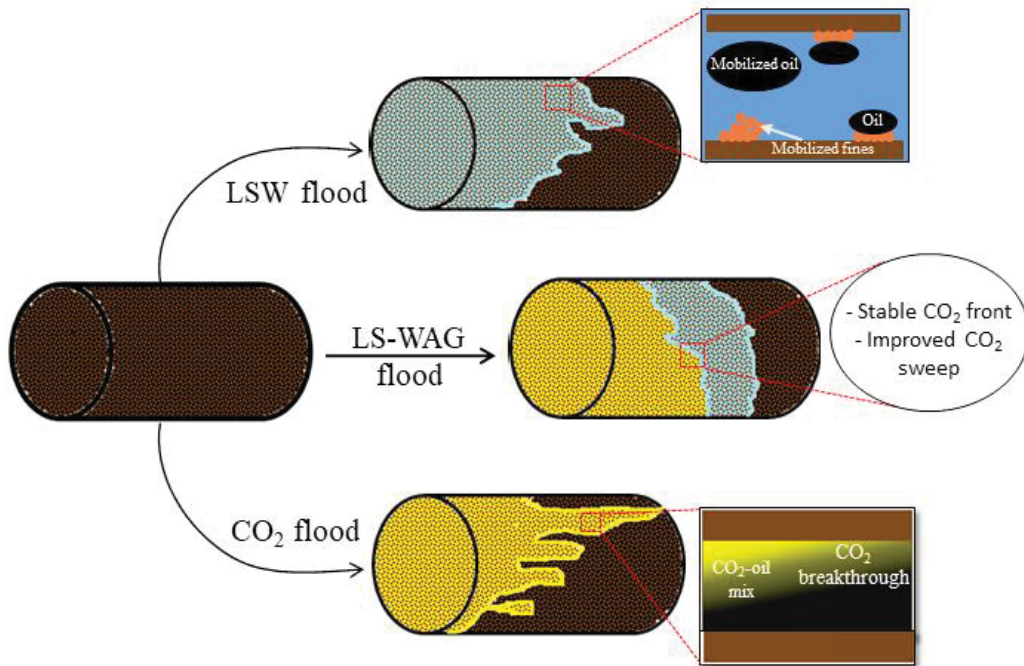
Tushar Sharma[†,*]

[†]Department of Petroleum Engineering, Rajiv Gandhi Institute of Petroleum Technology Jais,

Bahadurpur, Mukhetia More, Harbanshganj, Amethi, Uttar Pradesh-229304, India

[#]School of Engineering, University of Aberdeen, Aberdeen AB24 3UE. United Kingdom.

*Corresponding Author.

E-mail address: Tushar Sharma: tusharsharma.ism@gmail.com, Tel.: +91-7080044156

1

Graphical abstract

Mobilized oil

Oil

Mobilized fines

LSW flood

LS-WAG flood

- Stable CO_2 front
- Improved CO_2 sweep

CO_2 flood

CO_2-oil mix

CO_2 breakthrough

2

1   **Abstract**

2   CO_2 utilization for oil recovery applications is often impacted by the challenges such as

3   viscous fingering and its premature breakthrough. Injection of slugs of water-alternating-gas

4   (WAG) generally aims to overcome these challenges though the control of CO_2 mobility.

5   Moreover, the oil recovery potential of WAG is largely dependent on the injection water salinity

6   and the subsequent CO_2 dissolution and storage. Therefore, the effect of varying salinity (0-4

7   wt% NaCl) on CO_2 loading capacity of water is investigated in this study, at two test

8   temperatures of 323 K and 363 K and three confining pressures of 4, 8, and 12 bar, and

9   subsequently, the flooding experiments were performed to find the low salinity (LS)-WAG

10   process suitability in oil recovery applications from porous sandstone rocks. The inclusion of salt

11   was found to significantly affect CO_2 loading capacity of water. At higher NaCl concentration (4

12   wt%), CO_2 loading decreased by 50% as demonstrated by absorption kinetic study. LS-WAG

13   suggested maximum oil recovery 55-58% of original oil in place for water salinity of 2 wt%

14   NaCl at both the test temperatures. Increment in pressure had a positive impact on CO_2 loading

15   while increasing temperature showed reverse behavior. As a result of LS in WAG and kinetic

16   adsorption study, it is anticipated that the reduction in water salinity is a favorable factor in the

17   CO_2 storage and oil recovery performance of CO_2 injection. The instance of CO_2 injection was

18   also varied for LS-WAG process and its effect on oil recovery from sand-packs was reported. Oil

19   recovery results demonstrated that WAG was similarly effective in all the stages of the injection

20   cycle as long as water salinity remained lower than 2 wt% NaCl. Based on the findings in this

21   study, it is recommended to implement the WAG in conjunction with low salinity water (LSW)

22   in moderate saline conditions, which is of key importance for various applications where water

23   salinity differs on a large scale.

1   **Keywords**: - CO_2 Storage; LSW; Oil Recovery; Sandstone; Water Flooding; WAG

2   **1.   Introduction**

3   CO_2, as a greenhouse gas, is becoming a global threat for human health and environment

4   as its atmospheric concentration has already crossed the permissible limit of 350 ppm (Zhang et

5   al., 2016). The efforts seeking its atmospheric reduction are receiving widespread attention in

6   recent times. One of the methods is to utilize CO_2 on large scale for underground storage and the

7   oil recovery optimization, where CO_2 is expected to create enough miscibility with trapped oil

8   and mobilize its lighter hydrocarbon components towards surface (Chaturvedi et al., 2018;

9   Chaturvedi et al., 2019a; Honarvar et al., 2017; Ruidiaz et al., 2018). However, CO_2 being the

10   lighter gas than the crude oil, results in its early breakthrough due to bypassing and the viscous

11   fingering effects. This significantly reduces efficiency of CO_2-geological storage, and volumetric

12   sweep efficiency (Cao and Gu, 2013; Farzaneh and Sohrabi, 2015; Kargozarfard et al., 2019).

13   Water alternating gas (WAG) is the most popular method where premature breakthrough of CO_2

14   is controlled by the injection of water on regular intervals (Mahzari et al., 2019; Yu et al., 2019;

15   Zhao et al., 2015). The water column gets sandwiched between two subsequent CO_2 injections

16   and it helps to increase the residence time of CO_2 in porous media. Moreover, application of

17   water in this way forces CO_2 to reach the trapped oil in pore throats. Han and Gu (2014), in their

18   work explored the role of CO_2 slug size (0.125, 0.25, and 0.5 PV) and gas-water slug ratio (1:1,

19   1:2, and 2:1) in tight sandstone cores (Bakken) exhibiting a porosity of 8-10% and permeability

20   of 0.1-1 mD. They concluded that the use of smaller CO_2 slugs (0.125 and 0.25 PV) was

21   favorable for oil recovery and CO_2 utilization. In an experimental study of Seyyedi et al. (2018),

22   WAG injection (carbonated water) in sandstone core suggested 16% higher oil recovery when

23   compared to sole water flooding.

4

Thus, compared to sole CO_2, WAG process is more promising to make CO_2 injection remarkable for miscibility with crude oil and geological storage (Chaturvedi et al., 2020; Dang et al., 2016; Kumar and Mandal, 2017; Mahzari et al., 2019; Seyyedsar et al., 2016).

Another important development in effective utilization of injected water is the addition of salts in low concentrations, in the process called low saline water (LSW) injection. Several studies observed that the injection of low salinity brine helps to achieve higher incremental oil recovery (Al Harrasi et al., 2012; Brady and Krumhansl, 2012; Nasralla and Nasr-El-Din, 2014; Shaddel et al., 2014; Shojaati et al., 2017; Yang et al., 2016). Sharma and Filoco (2000) suggested that the use of low-salinity brine, as connate fluid, alters the wettability of the rock from a water-wet to a mixed-wet surface and contributes to an increase in oil recovery. LSW studies have been performed in both sandstone, and carbonate reservoirs where incremental oil recovery was mainly attributed to permeability modification of the rock surface (Austad et al., 2010; Yousef et al., 2011). Also, LSW can destabilize the extant equilibrium initially present in the rock-oil-brine system in the reservoir resulting in the increased oil recovery (Sheng, 2014). However, the primary mechanism behind salt interaction and its role on oil recovery remains unclear as researchers have debated physical (fines migration and detachment) and chemical aspects (interfacial tension and wettability alteration) as the dominating factors (Hamon, 2016). Literature studies on LSW have shown an increase in oil recovery by 8-20% over conventional water flooding. In addition, water-induced swelling of shale particles can be reduced by tuning the concentration of salt ions, which will make shaly-sandstone (an unconventional rock) more productive through the improvement in its petro-physical properties (Chaturvedi et al., 2019b). As compared to other EOR methods, LSW is environmental friendly and does not consist of expensive or harmful chemicals (Lee et al., 2019; Rostami et al., 2019).

It is now widely believed that the hybrid water injection such as LSW has the potential to improve oil recovery. Since LSW is a more advanced method than the conventional water flooding alone, it is possible to combine it with the WAG process where low salinity water flooding is expected to affect the pore structure during CO_2 injection and storage. It can help to improve the conformance performance of CO_2 by shutting off high conductivity zones and divert CO_2 towards the unswept zones (Dang et al., 2014). It is also essential to investigate the injection sequence of CO_2 and saline solution which can help to optimize the volume of gas and its handling costs. Otherwise, a significant quantity of CO_2 can be lost or get trapped in porous media, which may result in a negligible contribution to incremental oil recovery. Despite the vital importance of WAG process globally, LSW interaction with CO_2 (as an integrated EOR method, LS-WAG) for CO_2 dissolution in salt medium and oil recovery applications have been discussed in limited literature as far as we are aware. Effect of variable salinity on WAG process was first explained by Kulkarni and Rao (2005). Their core flooding experiments reported that LS-WAG acts as a better sweeping agent than a conventional WAG. Two types of brines, synthetic: 5 wt% NaCl solution and original: multi-component brine from a reservoir in West Texas, were used in their study. Besides, a range of the volume of slug size i.e. 0.2-0.6 PV was explored where 0.6 PV provided maximum resultant oil recovery. Recently, Teklu et al. (2016) studied the effect of CO_2 and low saline injection (diluted formation brine) for oil recovery from low permeability sandstone and carbonate cores. For both the cores, the incremental oil recovery of LS-WAG was 15-25% higher than conventional water flooding. However, a comprehensive study investigating the role of salt on efficacy of LS-WAG injection in sandstone reservoir is yet to be performed as far as we are aware.

In this study, we investigated the effect of varying salinity (0-4 wt% NaCl) on CO_2 loading capacity of water at the two different test temperatures of 323 and 363 K and three confining pressures of 4, 8, and 12 bar. CO_2 loading tests were performed to ascertain the viability of saline solution in carrying CO_2 in dissolved form and explore its role as CO_2-enriched LSW injection. For each of the solutions, the rate of CO_2 loading was determined using a first-order kinetics equation. This study also aims to investigate the viability of LS-WAG for EOR applications in a synthesized porous sand-pack environment at different test conditions. In each experiment, the injection of water of different salinity (0-4 wt%) was followed by CO_2 slug of different pore volume (PV) at a test temperature of 323 and 353 K. Finally, LS-WAG injection was performed by varying the instance of CO_2 injection and its effect on resultant oil recovery is reported accordingly.

2. Experimental Section

2.1. Methodology for the measurement of Carbon Capture in the saline aqueous phase

The experiments performed in this study used a commonly available salt, (Sodium Chloride-NaCl) of 99.5% purity in powder form. DI water was used to prepare the saline solutions (electrical conductivity of water = 0.0054 mS·cm^{-1}). CO_2 cylinder of the highest purity (99.99 %) was used for absorption and oil recovery runs.

The amount of CO_2 absorption (in moles/kg of solvent) in the saline solutions was measured using a well-established approach (Chaturvedi et al., 2018; Haghtalab et al., 2015; Haider et al., 2018). First, the confining pressure of 4, 8, or 12 bar (applied on the CO_2 molecules in the reservoir cell) was established using the pressure gauge and was used to calculate the number of CO_2 moles initially in the reservoir cell.

1    $n_{CO2}^i = \dfrac{P_i \, (V_{res})}{Z_{CO2}^i \, R \, T_{eq}}$

2   (1)

3   In Eq (1), n_{CO2}^i is the moles present in the reservoir cell, P_i is the initial confining

4   pressure, V_{res} is the volume of the gas in the reservoir (15 ml), R is the standard gas constant, T_{eq}

5   is the equilibrium test temperature and Z_{CO2}^i is the compressibility factor. At established

6   equilibrium conditions, the final value of pressure on the gauge was used to establish the no. of

7   CO_2 moles left unabsorbed in the cell using Eq. 2.

8    $n_{CO2}^{eq} = \dfrac{P_{eq} \, (V_{cell} - V_S)}{Z_{CO2}^f \, R \, T_{eq}}$ (2)

9   In Eq. 2, n_{CO2}^{eq} is the unabsorbed number of CO_2 moles in the equilibrium cell, V_s is the

10   volume of saline solution (i.e. 10 ml) which was measured and placed in equilibrium cell, P_{eq} is

11   the final value of pressure (equilibrium), and Z_{CO2}^f is the compressibility factor at equilibrium

12   conditions. To find out the number of CO_2 moles absorbed in the saline solutions, the difference

13   between the two obtained values from both Eqs. (1 and 2) is taken.

14    $n_{CO2}^{abs} = n_{CO2}^i - n_{CO2}^{eq}$ (3)

15   While the aforestated equations have been used to establish the amount of CO_2 which can

16   be absorbed (loaded) in a solution, it is also essential to determine the rate at which CO_2 is

17   absorbed (loaded) in the solution. The rate of absorption at an instance "t" can be estimated using

18   the relation between the gas concentration at equilibrium (n_e) and bulk gas concentration (n_t).

19   This relation has been expressed as

20    $\dfrac{dn}{dt} = k(n_e - n_t)$ (4)

Eq. 4 can also be written as:-

$$\ln \frac{(n_t - n_e)}{(n_o - n_e)} = -kt$$

(5)

Here, n_t is the CO_2 moles at time t, n_o is the original number of CO_2 moles at the start of the experiment, n_e is the CO_2 moles remaining at equilibrium and k is the absorption rate constant. A graph between $\ln \frac{(n_t - n_e)}{(n_o - n_e)}$ and t is plotted and the value of k is estimated by calculating the slope of the graph.

2.2. Determination of Interfacial Tension for CO_2-H_2O-salt system

Interfacial tension (IFT) between CO_2-H_2O-salt systems (0-4 wt%) was determined using pendant drop method. Conventionally, the pendant drop method is widely used in IFT measurements because of its flexibility and highly convenient (Arif et al., 2016). In pendant drop method, a small volume of the aqueous phase (either pure water or 1-4 wt% NaCl brine) is extruded from a thin needle in form of a droplet into CO_2, maintained at the desired pressure and temperature conditions. To determine IFT, the recorded droplet shape is analyzed at static conditions. Under these conditions, the shape of the droplet is dictated mainly by the balance between gravity and the extent of surface forces (Adamson and Gast, 1997). The main equation dictating the drop shape related to the liquid-gas interfacial tension is the Young-Laplace equation of capillarity.

$$\gamma_{(CO_2 - brine)} = \frac{\Delta \rho g}{(\beta k_{apex})^2}$$

(6)

1   Here, $\Delta\rho$ defines the difference in density between the gas and liquid, g is the

2   acceleration due to gravity, β is the dimensionless shape parameter and k_{apex} is used to define the

3   interface curvature at the apex point in the drop (Georgiadis et al., 2010).

4   The experimental set-up, as depicted in Fig. 1, consists of a cell (length and breadth = 6

5   cm, height= 10 cm) with glass windows (diameter 3 cm and distance of radii from top= 4 cm) cut

6   on either sides. The diameter of the inner needle was 1/8 inches. A light source was mounted on

7   one window. A camera was used to take the images of the rapidly forming droplet. The pressure

8   was maintained in the cell using a CO_2 cylinder and measured using a pressure transducer. The

9   temperature in the cell was maintained using a heating jacket and measured using a

10 thermocouple. The fluid was injected into the cell using a syringe pump. The attached camera

11 recorded several images, which were used to calculate the IFT through the well-established

12 method, pendent drop analysis method (Alvarez et al., 2009; Arif et al., 2016).

13 *2.3. Sand-pack preparation and flooding experiments*

14 To mimic the oil reservoir, a sand-pack was prepared using sand obtained from a

15 commercial vendor. Firstly, sand was carefully cleaned and dried at high temperatures to remove

16 any contaminants (Goswami et al., 2018). To characterize the sand particles, scanning electron

17 microscopy (SEM) and XRD (X-ray diffraction) analysis were performed. The results of SEM

18 and XRD analysis are provided in our previous studies (Chaturvedi et al., 2019b; Goswami et al.,

19 2018). From the obtained micrographs of SEM, it was established that the sand particles used

20 were of the size 200-380 mm. From the XRD analysis, it could be established that the

21 constituents of sand were quartz (88 wt%), kaolinite (6 wt%), feldspar (2 wt%), and chlorite (1

22 wt%). The presence of kaolinite is essential as the release of kaolinite is one of the key

10

1 mechanisms for LSW performance. The properties of the crude oil used in the study are provided

2 in Table 1.

3   The sand-packs were prepared manually in a sand-pack holder of length: 61 cm and

4 diameter: 3.80 cm. Slowly, both sand and the saturating medium were added to the sand-pack

5 holder and the mixture was continuously rammed with a special ramming rod. This entire

6 process was carried out until the entire sand-pack holder was full of saturated sand. The leftover

7 amount of water/saturating medium was then measured using the graduated cylinder and the

8 difference was noted. The water/saturating medium occupies the interstitial pore spaces between

9 the sand-grains termed as the pore-volume (PV) of the sand-pack. To determine the porosity, the

10 obtained pore volume is divided by the bulk volume of the sand-pack holder. Permeability is the

11 ease with which a fluid can flow in the porous medium. To estimate the permeability of the

12 synthesized sand-pack, the sand-pack was flooded with DI water at a constant flow rate (30 ml/h)

13 and the resistance to flow was recorded (Sharma et al., 2016). The resistance to flow is the

14 difference in pressure which was observed at the inlet and outlet of the sand-pack during the

15 fluid flow is referred to as the pressure drop (ΔP). Using Darcy's law, the values of pressure drop

16 are used to ascertain the permeability values (Sharma et al., 2016). The process was repeated

17 thrice for every sand-pack to establish repeatability and obtain accurate values of permeability.

18   A schematic of the experimental set-up used to perform the oil recovery experiments is

19 presented in Fig. 2. The experimental set-up of oil recovery test consisted of a CO2 cylinder, a

20 sand-pack holder (with an electrical heating jacket and temperature controller), two syringe

21 pumps, three high-pressure fluid accumulators, flow control values, and a measuring cylinder.

22 After the synthesis of the sand-pack, it was left untouched for 2 hours to ensure that the desired

23 test temperature was uniformly achieved throughout the sand pack. The fluids (water, saline

solutions, crude oil, CO_2 and chase water) were injected using the syringe pumps at very low flow rates to ensure that viscous fingering does not take place. The oil recovery experiments were carried out by following the well-established procedure (Chaturvedi et al., 2019a; Goswami et al., 2018; Sharma et al., 2016). To establish 100% water saturation in sand-pack, water was injected at a constant flow rate of 30 ml/hr. This was achieved by obtaining a steady stream of the saturating medium at the outlet. Crude oil is then injected at the 30 ml/hr until no further amount of crude could be retained in the sand-pack. The original oil in place (OOIP) was the amount of crude oil retained inside the sand-pack. The initial oil saturation (S_{oi}) of the sand-pack can be ascertained by establishing the percentage of OOIP in the pore volume. Using the difference between the initial pore volume and the established OOIP of the sand pack, the irreducible water saturation (S_{wi}) can be calculated. Below S_{wi}, no further amount of water can be reduced in the sand-pack.

$$S_{oi} = \frac{OOIP}{PV} * 100 \qquad (7)$$

$$S_{wi} = 1 - S_{oi} \qquad (8)$$

The recovery of oil was then carried out using the injection fluids until 5 PV of fluid had been injected. In the experiments where the role of WAG was being explored, a slug (0.3 PV) of CO_2 gas (performed at 60 ml/hr) was injected after 2 PV of injection and was followed up by a chase flood (performed at 60 ml/hr) till the total injection volume reached 5 PV. The displaced oil was carefully measured to establish the quantum of oil recovery using the used injection fluid. The percentage (%) of displaced oil was calculated using Eq. 9.

$$Displaced\ oil\ (\%) = \frac{OilCollected}{OOIP} * 100 \qquad (9)$$

3. Results and Discussion

1   In this section, the initial CO_2 loading capacity of the various saline solutions would be

2   investigated under a range of confining pressures and temperatures. This would be followed by a

3   discussion on the absorption kinetics of CO_2 in the saline solutions and how that would impact

4   the applicability of saline solutions as carbonated fluids. Finally, the flow behavior and oil

5   recovery results of low salinity water in conjunction with CO_2 injection are provided to ascertain

6   the efficacy of combined LS-WAG in oilfield applications.

7   *3.1. Molality, salting out and kinetics results for CO_2 absorption*

8   The primary mechanism for gas dissolution in water varies for different gases. Nonpolar

9   gases like the hydrogen (H_2) and oxygen (O_2) dissolve in an aqueous solution only as gas

10   molecules. However, for polar gases like carbon dioxide (CO_2) or sulfur dioxide (SO_2), the

11   dissolution takes place in different ways. For CO_2, while the dominant mechanism behind gas

12   absorption is physisorption (CO_2 trapped in form of bubbles encapsulated by layers of water), a

13   small part of the gas molecules react with water to produce H_2CO_3 (carbonic acid, a very weak

14   acid) which further partially dissociates into HCO_3^- ions. Thus, in water, CO_2 can exist not only

15   as the complete CO_2 molecules but also as H_2CO_3 molecules, HCO_3^- ion, and CO_3^- ions. This

16   absorption is estimated in the form of CO_2 moles which have been encapsulated in a specified

17   unit of solvent (water in this study). The absorption of CO_2 in the solutions of varying salinity (0-

18   4 wt%) was estimated using Eq. 3. This data was estimated for each of the 3 confining pressures

19   (4, 8, and 12 bar) at two test temperatures (323 and 363 K) in form of CO_2 molality (moles of

20   CO_2 absorbed in a solvent) and depicted in Fig. 3. The CO_2 loading experiments were repeated 5

21   times and the deviations have been plotted as error bars in Fig. 3. It is evident from these results

22   that the inclusion of salt markedly decreases the absorption of CO_2 in a solvent. While the effects

23   are less evident in lower salt concentrations (1, 2 wt%), at higher wt%, CO_2 absorption has been

found to reduce significantly. The fall in the absorption is primarily due to the dissolution of salts in the water which increases its density. At high salinity, the presence of ions is high and this increases the saturation level of the base fluid (in our case, water). The solubility decreases as the salinity increases due to the increased salting-out effect (Carvalho et al., 2015; Messabeb et al., 2017). This salting-out effect can be defined as the relative reduction in the amount of CO_2 absorption in any salty solution compared to the amount of CO_2 absorption, observed in pure water.

From Fig. 3, it is also evident that at higher ion saturations, the CO_2 is salted out by the dissolved salts, hence, gas solubility is less. Alternatively, it can be said that the involvement of water molecules with salt ions decreases the already weak affinity of CO_2 molecules to water and reduces the dissolution of CO_2. The salting-out effect exhibited by the NaCl salts on CO_2 solubility in water has been found to depend on the charge of ions, salt concentration, and temperature of the solution (Carvalho et al., 2015; Pérez-Salado Kamps et al., 2006). At times, the ion and solute interactions are shielded by a hydration shell which also influences gas solubility (Carvalho et al., 2015).

Even at higher pressures, the absorption markedly decreased in higher salinity solution. However, the effects were less pronounced at higher pressures. While the absorption halved at 4 bar when comparing 4 wt% saline solution with pure water, it fell by only 35% (from 0.221 mol/kg to 0.144 mol/kg) at 8 bar and by 32% (from 0.362 mol/kg to 0.25 mol/kg) at 12 bar. This proves that at higher pressures, the CO_2 absorption is more dominated by confining pressure rather than salt effect. These results are closer to the data observed in the work of Rumpf et al. (1994) where CO_2 absorption was found to be 0.42 mol/kg at 20 bar and 313 K. With increasing temperature, the absorption decreased for all the solvents. These results follow a similar trend

established by Weiss (1974) who compiled the solubility of CO_2 in saline solutions between 272 and 313 K. An increase in temperature is found to increase the kinetic energy of a gas. It is expected that an increase in kinetic energy will result in more motion in the gas molecules. This caused them to break their intermolecular bonds, aiding them in escaping from the solution. Hence, a lesser amount of CO_2 is absorbed by all the solutions at a higher temperature.

To quantify absorption (loading) of CO_2 in the aqueous solutions, the value of the rate of absorption (k) was determined using the method established in Section 2.2. The results were plotted in the form of a graph represented in Fig. 4. The value of k is determined by the slope of the graph. Higher value of k indicates that faster absorption takes place. A faster rate of CO_2 absorption (loading) is beneficial for the industry as less amount of energy will be expended and more solutions can be prepared at the same time interval. Fig. 4 also indicates that the inclusion of salt ions has reduced the rate of absorption of CO_2 in solution. The effect on the rate of absorption is negatively influenced by salt concentration. 4 wt% saline solution exhibited the lowest rate of CO_2 absorption. The values of CO_2 absorption kinetics for water follow the same trend established in previous work (Chaturvedi et al., 2018). All saline solutions exhibited lower CO_2 absorption and kinetics at both temperatures. Moreover, the solubility mechanism of CO_2 in water becomes significantly less effective in more saline formations due to the effect of salinity on the solubility of CO_2. The lower CO_2 solubility in brine will promote oil swelling and reduction in oil viscosity, instead of remaining entrapped in water for oil recovery enhancement objective alone (Al-Abri et al., 2019). Hence, WAG studies were carried out using all saline solutions where instead of CO_2 being absorbed in the solution, it is injected as a gas slug (0.3 PV).

3.2. IFT determination of CO_2-H_2O-salt system

1   One of the key constraints in subsurface CO_2 injection is the need to know the interfacial

2   tension between CO_2 and brine. Using process stated in section 2.3, IFT was determined by the

3   pendant drop method and the results have been presented in Fig. 5. For CO_2-water, IFT was

4   determined as 42 mN/m at 4 bar and 323 K. IFT was found to reduce from 33 to 31 mN/m with

5   pressure increase from 8 to 12 bar, respectively. From Fig. 5, it was noted that effects of

6   buoyancy become predominant with increase in pressure. This can be attributed to the phase

7   density difference between external and droplet phase, which was found to decrease with

8   increasing pressure. This leads to the formation of larger droplets (Fig. 6) before they become

9   too heavy to be supported by the forces at the needle, altering IFT of CO_2-water interface. The

10   higher pressure inside the cell can support a greater volume of injected fluid before it detaches

11   from the needle (Fig. 6). This decrease in IFT can be attributed to increased solubility of CO_2 in

12   water with increasing pressure (Bachu and Brant Bennion, 2009; Chaturvedi et al., 2018). To

13   ensure that values were repeatable even when different levels of fluids existed in the cell, the

14   images were captured at separate intervals and the IFT was found to be reproducible with only

15   minor variations (Fig. 5).

16   With the addition of salt, it was observed that IFT between CO_2 and water increases. IFT

17   for 1 wt% NaCl solution was 43 mN/m at 4 bar which was determined to be 46 mN/m for 4 wt%

18   NaCl solution. A similar trend was repeated for all pressure values when the inclusion of salt

19   increased the IFT when compared to only pure water-CO_2. These results indicate a pre-

20   established trend whereby on the addition of any salt i.e. NaCl, KCl, $CaCl_2$, or $MgCl_2$, they alter

21   the physical properties and phase behavior, particularly the IFT of aqueous systems

22   (Aggelopoulos et al., 2011; Li et al., 2014). Our findings were corroborated by previous studies

23   that have established that the gas-water IFT increases with the introduction of salt in the system.

1   This is mainly due to the ion distribution present in bulk-aqueous phase and the interfacial

2   region. In past studies, it has been observed that the surface tension values for different salt

3   solutions were greater than those observed in solutions without salt under similar conditions

4   (Johansson and Eriksson, 1974; Pereira et al., 2017). The authors reported, through their

5   understanding of an electrolyte free layer and application of Gibbs adsorption equation, that IFT

6   increase may be related to the depletion of ions at the interface. Similar was reported by Hey et

7   al. (1981) who found that the change in IFT was directly proportional to the enthalpy of

8   hydration of ions (i.e. attraction to water) and it was suggested that the ions, instead of being

9   partially hydrated at the interface, preferred to be fully hydrated in bulk phase. Conventionally,

10   compared to anions, cations display a stronger affinity to water molecules. This predictably

11   means that at the interface, the cations are strongly repelled. Hence, the resulting cation

12   hydration leads to an increase in the ratio of cation charge to cation surface area, increasing their

13   impact on IFT. Similarly, the density increase of the aqueous phase and gas solubility decrease

14   (salting-out effect) also influences the fluid IFT (Carvalho et al., 2015; Messabeb et al., 2017).

15   This is because the average molecular weight of the solution (the aqueous phase) increases with

16   the addition of salts, this increasing density which further increases the density difference

17   between phases ($\Delta\rho$) (here water and CO_2). With the increase in the temperature, the CO_2-water

18   IFT was found to increase for all solutions [Fig. 5b] leading to the reduction of CO_2 solubility in

19   water (Bachu and Brant Bennion, 2009). The available data shows that IFT of CO_2-fluid

20   interface strongly depends on solubility effects of CO_2 in the system. With increasing pressure (8

21   to 12 bar), IFT decrease is the indication of enhanced CO_2 solubility in solution (Aggelopoulos et

22   al., 2011), which was not observed at high temperature (353 K) during NaCl increase from 2 to 3

23   wt%. It is clear from results that IFT decrease at low pressures is steeper as observed during 4-8

bar while further increase (8-12) could not produce enough decrease in IFT values. Thus, at elevated pressures, IFT is expected to show insignificant reduction as CO_2 solubility in brine may decrease as demonstrated in literature (Aggelopoulos et al., 2011). In addition, it can be expected that increasing temperature affected the solubility potential of CO_2 in brine as it has been established that IFT dependence on temperature is more complex than that of pressure (Bachu and Bennion, 2009a; Bachu and Bennion, 2009b). Therefore, at 353 K, it is possible that pressure increment of 4 bar (8-12 bar) was not enough to reduce the effect of temperature on CO_2 solubility in brine of 2 wt% NaCl. However, at 4 wt% NaCl, the amount of electrolytes was enough in the solution that probably became sufficient to dominate the effect of temperature resulting IFT showed the normal decrease. Similarly, no change in IFT was observed for 3 wt% NaCl solution for pressure increment from 8 to 12 bar at 353 K. However, authors further agree that the effect of salinity for water-CO_2 system at high temperature and pressure is not understood well in this study and may require more extensive investigations.

3.3. Core flooding experiments

The saline solutions were then used in oil recovery experiments to establish their efficacy in oil recovery studies. The nomenclature, porosity, and permeability of the oil recovery runs (1-15) have been provided in Table 2. The use of the saline solutions as saturating medium slightly reduced the porosity (from 33.2% for pure water to 29.84% for 4 wt% saline solution). The porosity and permeability of the sand-packs were fairly reproducible in the range of 32 ±2% (porosity) and 750±66 md (permeability). The irreducible water saturation was found to be 32 ± 1.3% OOIP (Table 2).

3.3.1. Time to breakthrough

18

The time taken for the first instance of CO_2 bubble to appear at the outlet (CO_2 breakthrough) after the start of chase water flooding was carefully observed and the results, as a function of an oil recovery run, are presented in Fig. 7. These results indicated the oil recovery studies at varying temperature and time of CO_2 injection. As the sand-pack had been completely saturated with the saturating fluid (which removed any entrapped air), it is unlikely that any other gas apart from CO_2 was already present in the sand-pack. The emergence of the bubble was also confirmed by checking the amount of fluid in the cylinder present at the outlet. It was observed that the emergence of the CO_2 bubble did not increase the amount of fluid present in the cylinder consummate with the rate of injection.

In porous media, CO_2 breakthrough greatly depends on the fluid present ahead of its front and the fluid present behind it. The injected CO_2 came very early (within 9 min) when water flooding was performed in a sand-pack where no fluid was initially present inside the pore throats. Here, the injected water easily pushes the lighter CO_2 and CO_2 does not have any fluid (water/oil) inside to resist its frontal movement. Since CO_2 was lighter than water, CO_2 breakthroughs within 9 min after water flooding. 19 min of breakthrough time was achieved when both water and oil were initially present in the sand-pack, a case of secondary oil recovery. The increase in retention time can be attributed to the fact that CO_2 movement was restricted by the present fluids in pore throats. As a result, CO_2 is tended to interact with both water and oil present inside the sand-pack. Some amount CO_2 is expected to show solubility in water through physical equilibria (Haghtalab et al., 2015). The remaining amount of CO_2 will either be forced into the oil or stay trapped in the sand-pack between the water interface. However, an increase in oil recovery on CO_2 injection indicates that some amount of CO_2 was indeed solvated in the crude oil, which reduced its density and viscosity and made it more conducive for production.

When the chase fluid was 1 wt% NaCl solution, the time to breakthrough reduced to 18 mins. Further increasing the salt concentration, it was observed that the time to breakthrough decreased continuously from 17 mins when flooding with 2 wt% NaCl solution to just 14 mins when 4 wt% NaCl solution was used. The reduction in time taken for CO_2 to breakthrough can be explained by the salting-out effect exhibited by salt concentration on CO_2 absorption in saline solutions (Carvalho et al., 2015; Messabeb et al., 2017). The inclusion of salt reduces CO_2 intake capacity of the solution, forcing CO_2 to move further towards the outlet which in turn contributes to higher participation in oil recovery. At high salt concentration, negligible CO_2 loading was observed and hence, the time to breakthrough was least. This can be further understood by observing the role of residual water in the efficacy of CO_2 injection process which performs comparatively worse in the presence of higher connate water as more CO_2 is trapped with water, instead of oil (Chaturvedi et al., 2019a). The use of saline water reduces some of the affinity of CO_2 for water and promotes higher participation of CO_2 in oil recovery.

With the increase in temperature of the reservoir, it was observed that the time for CO_2 breakthrough was slightly reduced (from 19 min for water at 323 K to 18 min at 353 K). Similar reductions were observed in 1 wt% NaCl solution (from 18 to 17 min) and 3 wt% NaCl solution (from 15 to 14 min). The most significant difference was observed in the 4 wt% salt solution where the time is taken for CO_2 to breakthrough reduced from 14 min (at 323 K) to 12 min (at 353 K). This reduction can be attributed to the lower absorption of CO_2 in fluids at higher temperatures due to their increase in kinetic energy (Chaturvedi et al., 2018). Also, at higher temperatures, the density and viscosity of fluids reduce which makes it easier for the CO_2 to finger through the entire length of the sand-pack (Goswami et al., 2018). This reduction in CO_2

loading together with salting-out effect greatly reduces the time taken for CO_2 to a breakthrough

in the saline solutions at higher temperatures.

When the time of CO_2 injection was varied (i.e. injection of CO_2 slug after 1 PV, 2 PV

and 3 PV of saline water injection, respectively) in runs 13-15, the time taken for CO_2 to

breakthrough was observed to be between 18 min (for CO_2 slug injection after 1 PV and 2 PV of

flooding) and 19 min (when CO_2 slug was injected after 3 PV of flooding). Since no CO_2 was

injected in runs 11 and 12, no values of CO_2 breakthrough have been provided for them. Based

on these results, it can be deduced that increasing salt concentration reduces the amount of time

spent by the CO_2 in the sand-pack to breakthrough. Hence, an implementation of CO_2 in

conjunction with high salinity water for oil recovery is not recommended especially in the

subsurface CO_2 storage in the depleted produced zone combined with CO_2 EOR schemes.

3.3.2 Pressure drop studies

The injection of any fluid (water, saline solution or gas) in a porous medium generates a

resistance that is observed in the form of a pressure drop on the injecting mechanism (syringe

pump). To understand the oil mobilization potential and properties of injection fluids, it is

essential to continuously monitor the values of pressure drop (psi) throughout fluid injection. All

values of pressure drop (psi) vs fluid injected (PV) for runs 1-15 has been presented in form of

Fig. 8a (runs 1-5 at 323 K), 8b (runs 6-10 at 353 K), and 8c (runs 11-15 at 323 K and varying

CO_2 injection rates). During the initial water flooding (2 PV), for water (run-1), the value of

pressure drop remains closer to 2.3 psi, and very little fluctuation is observed until the slug of

CO_2 is injected. On the injection of CO_2, the pressure falls initially to 0.62 psi (at 2.25 PV) and

then increases to 1.14 psi (at 2.5 PV). Once, the maximum recovery of oil has taken place (at 3

PV), pressure drop falls to 2.1 psi and remains nearly constant until the completion of run-1. This

is due to the low viscosity of CO_2 that moves through the pores at ease during its injection (CO_2 slug). The pressure drop then gradually increased (2.42 psi for 1 wt% NaCl, 2.55 psi for 2 wt% NaCl solution, and 2.84 psi for 4 wt% solution) as the salt concentration is increased. Water viscosity increased with the addition of salts. In all gas slug injection cases (runs 1-10, 13-15), the recorded pressure drop declined. However, the pressure drop is not consistent in all cases (varying between 0.62 psi to 0.89 psi). A similar trend was observed during the intermittent low salinity water and gas flooding, analogous the work of Al-Abri et al. (2019). At higher temperature, the values of pressure drop reduced marginally for all solutions. During water injection at 353 K pressure drop reduced to 1.5 psi while the injection was carried out. Similarly, the recorded pressure drop values for 1-4 wt% NaCl solutions were 1.58, 1.64, 1.84, and 2.06 psi, respectively (Fig. 8b). This fall in pressure drop for all solutions can be attributed to solution viscosity which has an inverse dependence on temperature (Chaturvedi et al., 2019; Goswami et al., 2018). For run 11-15 (Fig. 8c), the values of pressure drop observed were similar to those observed in run 1-5 (Fig. 8b) whenever a CO_2 slug was injected following the 1, 2 or 3 PV fluid injection. Trend of similar pressure drops recorded even at different time of CO_2 injection confirm that CO_2 WAG will be effective at all stages of the water flooding which has also been confirmed by our oil recovery experiments. However, the CO_2 injection in earlier stages of the oil recovery process is recommended to avoid the water shielding of oil and obtain higher incremental oil recovery benefits.

3.3.2. Oil Recovery

The injection sequence adopted for oil recovery experimental runs 1-10 was: initial water/saline solution-flooding (2 PV) $\rightarrow$ injection of 0.3 PV CO_2 slug $\rightarrow$ final chase water/saline-solution flooding (2.7 PV). The results of the oil recovery were tabulated as a

function of the fluid injected and have been presented as Fig. 9(a-c). The first five oil recovery runs (1-5) were carried out at temperature 323 K using solutions of varying salinity (0-4wt%) and the results are presented in Fig. 9a. All experiments were stopped once total 5 PV of fluids had been injected in the sand-pack. In run 11, the injection of water was performed (similar to run 1) while in run 12, the injection of 1 wt% NaCl solution was performed. In runs 13-15, the injection of 1 wt% NaCl solution was performed by altering the time instance of CO_2 injection, i.e. a CO_2 slug (0.3 PV) was injected at the completion of 1, 2 and 3 PV of 1 wt% NaCl solution which was followed by chase water flooding till a total of 5 PV fluid had been injected in the sand-pack.

Based on the results analyzed in this study, it is observed that the inclusion of salt ions at a lower concentration in the injected water in conjunction with the injection of CO_2 gas resulted in the significantly higher incremental oil recovery. While 48% OOIP was recovered during WAG with pure water (run-1), the addition of 1 wt% NaCl in injection water yielded 55% OOIP (run-2). Further increase resulted in lower oil recovery: 58% using 2 wt% NaCl (run-3), 56% using 3 wt% NaCl (run-4), and 54% using 4 wt% NaCl (run-5). The incremental recovery during run-1 can be attributed to CO_2 that reduces the viscosity of oil through swelling and thereby, it increases mobilization. The use of LSW together with CO_2 injection further increased the oil recovery. This increase can be indirectly attributed to fines migration and wettability alteration due to LSW (Brady et al., 2015; Tang and Morrow, 2002). Al-Abri et al., (2019) also established that the dominant mechanism behind improved oil recovery in LS-WAG is the synergy between a multi-component ionic exchange (MIE) of Na^+ ions which causes wettability alteration (LSW) and partial miscibility of CO_2 (WAG).

1   At higher temperatures, while the oil recovery marginally increased to 49% OOIP for

2   WAG using pure water (run-6), it improved to 54% OOIP for 1 wt% NaCl solution (run-7).

3   Similarly, 55% (run-8), 53% (run-9) and 51% OOIP (run-10) was recovered when 2 wt%, 3 wt%

4   and 4 wt% NaCl water was injected, respectively (see Fig. 9b). The small increase in the oil

5   recovery observed during run-6 can be attributed to a reduction in the oil viscosity observed

6   when the test temperature is increased from 323 K to 353 K. A detailed discussion of the role of

7   temperature on oil recovery during the LSW flooding is provided in section 3.3.4. This was

8   followed by oil recovery runs from 11-15 where gas injection rates were varied (Fig. 9c). The

9   run 11 was performed using water while runs 12-15 were performed using 1 wt% NaCl solution.

10   Experimental run-11 resulted in 39% oil recovery. Additional 8% oil recovery (total 47%) was

11   obtained when 1 wt% NaCl was added in water (run-12). For LS-WAG, gas slug (0.3 PV)

12   injection resulted in 55% oil recovery after 1 PV (runs 13 and 14) and 54% oil recovery after 3

13   PV of low saline flooding (run 15). The observed results indicate that CO_2 injection will improve

14   oil recovery from a reservoir irrespective of its injection time i.e. after 1, 2 or 3 PV of low saline

15   flooding.

16   *3.3.4 Comparison of oil recovery*

17   To further delineate, the viability of low saline water flooding (LSW), a comparative

18   evaluation of the oil recoveries during the various experimental runs conducted in this study was

19   performed. The runs were compared with a baseline scenario and the following equation was

20   used-

$$IR\% = \frac{100 * (R_o - R)}{R_o}$$

Here, IR is the incremental oil recovery, R_o is the oil recovery observed in the base line scenario and R is the oil recovery observed in the test case. All units are %OOIP. The base line scenarios used to prepare the results were the oil recovery observed in run-1 (CO_2 and pure water flooding at 323 K), run-6 (CO_2 and pure water flooding at 353 K), run-11 (sole water flooding at 323 K) and run-12 (1 wt% NaCl flooding at 323 K). While base cases (R_o) for Fig. 10a are runs 1 and 6, the base cases for Fig. 10b are runs 11 and 12. The incremental oil recovery results (IR%) over the base cases are presented in Fig. 10. From the Fig. 10a, it is clear that the oil recovery improved for all salt concentrations at both temperatures. At 323 K, it was observed that compared to CO_2 and pure water flooding, the use of salt solutions increases the oil recovery significantly. The injection of 1 wt% NaCl solution (LSW) increased the oil recovery by 7%, while injection of 2 wt% NaCl solution suggested oil recovery increment of 10%. IFT between crude oil and saline solution is affected by the concentration of salts in the solution. Initially, IFT decreases with increasing salt concentration and then it achieves a minimum value at 2 wt% NaCl, where oil recovery was reported to be maximum (55% of OOIP). This is known as the critical salt concentration (CSC). Above CSC, IFT between crude oil/water systems starts to increase again. This resulted into the decrease in oil production (53% OOIP when 3 wt% NaCl was injected and 51% OOIP when 4 wt% NaCl was injected). From the results, it can be understood that CSC is around 2 wt% NaCl concentration (where oil recovery was highest). Thus, the oil recovery reduced with increasing salt concentration in the injection water (8% OOIP for 3 wt% NaCl and 6% OOIP for 4 wt% NaCl).

From IR results of runs 7-10 (with base case R_o, run 6) [plotted in Fig. 10a], it can be observed that oil recovery decreases with increasing temperature. Compared to 7% incremental oil recovery at 323 K, only 5% additional oil is produced when the test temperature increases to

353 K. Even for 2 wt% NaCl, the incremental oil recovery reduces from 10% to 6% at higher temperature. These results show that the effect of LSW is diminished at high temperature (Thyne, 2016). Temperature may negatively affect the geochemical interactions between the rock surface, reservoir brine, and crude oil causing a reduction in oil recovery (Mansi et al., 2020). According to Xie et al. (2017), while reservoir temperature and pressure have a direct bearing on oil recovery result of LSW, it is the effect of water chemistry (ions) that is most dominant on LSW. In Fig. 9c, the oil recovery observed during water flooding (for run-11) was 39% OOIP and oil recovery during 1 wt% NaCl saline flooding was 47% OOIP. These values were used to determine the relative performance of the runs 13-15 and the results have been presented in Fig. 10b. LSW improved the oil recovery by 8% (run 11 *vs.* run 12) while the use of LSW in conjunction with CO_2 further improved the oil recovery by 16% (1 wt% NaCl solution), 16% (2 wt% NaCl solution), and 15% (4 wt% NaCl solution). These observations also indicate that CO_2 and LSW have played a role in improving oil recovery and thus, it is highly recommended for EOR from depleted oil reservoirs.

4. Conclusion

In this study, the role of salt ions on CO_2 loading, kinetics, and oil recovery in form of low salinity water-alternating gas (LS-WAG) has been explored. CO_2 loading potential of saline solutions (0-4 wt% NaCl) was established using the pressure drop method in an equilibrium cell and the inclusion of salt ions was found to reduce the CO_2 loading in the confining fluid. At higher salt concentrations ($\geq$ 4 wt% NaCl), the addition of salt ions led to salting out of CO_2 and very little CO_2 was solvated in the solution. The inclusion of salt also decreased the rate of absorption of CO_2 in the solution. IFT between CO_2 and saline solutions was explored to further establish the role of salt on brine/CO_2 IFT. The inclusion of salt increased IFT as the CO_2-fluid

26

interface IFT strongly depends on the solubility effects of CO_2 in the system. Uniquely, a variation in CO_2 solubility is observed whereby it is found to increase on applying more pressure and decreases with an increase in temperature. CO_2 solubility also affects the IFT, which is proportionally altered in the opposite direction (i.e., decreases with decreasing pressure and increases with increasing temperature and water salinity). These results indicate that saline solutions are not good carriers of CO_2 and thus, their potential for use as carbonated solutions may be constrained due to lower CO_2 loading, delayed absorption and detrimental IFT. However, oil recovery tests carried out with CO_2 and LSW injected in sequence, improved oil recovery by 5-16%. The lack of solubility of CO_2 in saline water, indicated by a set of flow behavior studies further pushes more CO_2 towards the crude oil and in synergy with salt effect, improves oil recovery. Finally, a comparative analysis of sole water flooding and saline solutions, indicate that salt water is much more viable in oil recovery by giving higher recovery of oil in the varying injection and temperature conditions. Hence, the use of saline solutions of lower concentration (1 and 2 wt%) is recommended in conjunction with CO_2 injection for improving oil recovery from brownfield reservoirs.

Acknowledgments

References

Adamson, A.W., Gast, A.P., 1997. Physical chemistry of surfaces. Wiley.

Aggelopoulos, C.A., Robin, M., Vizika, O., 2011. Interfacial tension between CO_2 and brine (NaCl+CaCl$_2$) at elevated pressures and temperatures: The additive effect of different salts. Adv. Water Resour. 34, 505–511.

Al-Abri, H., Pourafshary, P., Mosavat, N., Al Hadhrami, H., 2019. A study of the performance of the LSWA CO_2 EOR technique on improvement of oil recovery in sandstones. Petroleum 5, 58–66.

Al Harrasi, A., Al-maamari, R.S., Masalmeh, S.K., 2012. Laboratory Investigation of Low Salinity Waterflooding for Carbonate Reservoirs, in: Abu Dhabi International Petroleum Conference and Exhibition. Society of Petroleum Engineers.

Alvarez, N.J., Walker, L.M., Anna, S.L., 2009. A non-gradient based algorithm for the determination of surface tension from a pendant drop: Application to low Bond number drop shapes. J. Colloid Interface Sci. 333, 557–562.

Arif, M., Al-Yaseri, A.Z., Barifcani, A., Lebedev, M., Iglauer, S., 2016. Impact of pressure and temperature on CO_2-brine-mica contact angles and CO_2-brine interfacial tension: Implications for carbon geo-sequestration. J. Colloid Interface Sci. 462, 208–215.

Austad, T., Rezaeidoust, A., Puntervold, T., 2010. Chemical Mechanism of Low Salinity Water Flooding in Sandstone Reservoirs, in: SPE Improved Oil Recovery Symposium. Society of Petroleum Engineers, Tulsa, OK.

Bachu, S., Brant Bennion, D., 2009a. Dependence of CO_2-brine interfacial tension on aquifer pressure, temperature and water salinity. Energy Procedia 1, 3157–3164.

Bachu, S.; Brant Bennion, D., 2009b. Interfacial tension between CO_2, freshwater, and brine in

the range of pressure from (2 to 27) MPa, temperature from (2 to 125) °C, and water salinity from (0 to 334000) mg·L^{-1}. J. Chem. Eng. Data 54 (3), 765−775.

Brady, P. V., Krumhansl, J.L., 2012. A surface complexation model of oil-brine-sandstone interfaces at 100°C: Low salinity waterflooding. J. Pet. Sci. Eng. 81, 171–176.

Cao, M., Gu, Y., 2013. Oil recovery mechanisms and asphaltene precipitation phenomenon in immiscible and miscible CO_2 flooding processes. Fuel 109, 157–166.

Carvalho, P.J., Pereira, L.M.C., Gonçalves, N.P.F., Queimada, A.J., Coutinho, J.A.P., 2015. Carbon dioxide solubility in aqueous solutions of NaCl: Measurements and modeling with electrolyte equations of state. Fluid Phase Equilib. 388, 100–106.

Chaturvedi, K.R., Kumar, R., Trivedi, J., Sheng, J.J., Sharma, T., 2018. Stable Silica Nanofluids of an Oilfield Polymer for Enhanced CO_2 Absorption for Oilfield Applications. Energy Fuels 32, 12730–12741.

Chaturvedi, K.R., Trivedi, J., Sharma, T., 2019a. Evaluation of Polymer-Assisted Carbonated Water Injection in Sandstone Reservoir: Absorption Kinetics, Rheology, and Oil Recovery Results. Energy Fuels 33, 5438–5451.

Chaturvedi, K.R., Singh, A.K., Sharma, T., 2019b. Impact of shale on properties and oil recovery potential of sandstone formation for low-salinity waterflooding applications. Asia-Pacific J. Chem. Eng. 14.

Chaturvedi, K. R., Trivedi, J., Sharma, T., 2020. Single-Step Silica Nanofluid for Improved Carbon Dioxide Flow and Reduced Formation Damage in Porous Media for Carbon Utilization. Energy 197, 117276.

Dang, C., Nghiem, L., Nguyen, N., Chen, Z., Nguyen, Q., 2016. Evaluation of CO_2 Low Salinity Water-Alternating-Gas for enhanced oil recovery. J. Nat. Gas Sci. Eng. 35, 237–258.

Dang, C.T.Q., Nghiem, L.X., Chen, Z., Nguyen, N.T.B., Nguyen, Q.P., 2014. CO_2 Low Salinity Water Alternating Gas: A New Promising Approach for Enhanced Oil Recovery, in: SPE Improved Oil Recovery Symposium. Society of Petroleum Engineers, Tulsa, OK.

Farzaneh, S.A., Sohrabi, M., 2015. Experimental investigation of CO_2-foam stability improvement by alkaline in the presence of crude oil. Chem. Eng. Res. Des. 94, 375–389.

Georgiadis, A., Maitland, G., Trusler, J.P.M., Bismarck, A., 2010. Interfacial tension measurements of the ($H_2O + CO_2$) system at elevated pressures and temperatures. J. Chem. Eng. Data 55, 4168–4175.

Goswami, R., Chaturvedi, K.R., Kumar, R.S., Chon, B.H., Sharma, T., 2018. Effect of ionic strength on crude emulsification and EOR potential of micellar flood for oil recovery applications in high saline environment. J. Pet. Sci. Eng. 170, 49–61.

Haghtalab, A., Mohammadi, M., Fakhroueian, Z., 2015. Absorption and solubility measurement of CO_2 in water-based ZnO and SiO_2 nanofluids. Fluid Phase Equilib. 392, 33–42.

Haider, M.B., Jha, D., Marriyappan Sivagnanam, B., Kumar, R., 2018. Thermodynamic and Kinetic Studies of CO_2 Capture by Glycol and Amine-Based Deep Eutectic Solvents. J. Chem. Eng. Data 63, 2671–2680.

Hamon, G., 2016. Low-Salinity Waterflooding: Facts, Inconsistencies and the Way Forward - OnePetro. Petrophysics 57.

Han, L., Gu, Y., 2014. Optimization of miscible CO_2 water-alternating-gas injection in the

bakken formation. Energy Fuels 28, 6811–6819.

Hey, M.J., Shield, D.W., Speight, J.M., Will, M.C., 1981. Surface tensions of aqueous solutions of some 1:1 electrolytes. J. Chem. Soc. Faraday Trans. 1 Phys. Chem. Condens. Phases 77, 123–128.

Honarvar, B., Azdarpour, A., Karimi, M., Rahimi, A., Afkhami Karaei, M., Hamidi, H., Ing, J., Mohammadian, E., 2017. Experimental Investigation of Interfacial Tension Measurement and Oil Recovery by Carbonated Water Injection: A Case Study Using Core Samples from an Iranian Carbonate Oil Reservoir. Energy Fuels 31, 2740–2748.

Johansson, K., Eriksson, J.C., 1974. γ and $d\gamma/dT$ measurements on aqueous solutions of 1,1-electrolytes. J. Colloid Interface Sci. 49, 469–480.

Kargozarfard, Z., Riazi, M., Ayatollahi, S., 2019. Viscous fingering and its effect on areal sweep efficiency during waterflooding: an experimental study. Pet. Sci. 16, 105–116.

Kulkarni, M.M., Rao, D.N., 2005. Experimental investigation of miscible and immiscible Water-Alternating-Gas (WAG) process performance. J. Pet. Sci. Eng. 48, 1–20.

Kumar, S., Mandal, A., 2017. A comprehensive review on chemically enhanced water alternating gas/CO_2 (CEWAG) injection for enhanced oil recovery. J. Pet. Sci. Eng. 157, 696–715.

Lee, Y., Park, H., Lee, J., Sung, W., 2019. Enhanced oil recovery efficiency of low-salinity water flooding in oil reservoirs including Fe^{2+} ions. Energy Explor. Exploit. 37, 355–374.

Li, Z., Wang, S., Li, S., Liu, W., Li, B., Lv, Q.C., 2014. Accurate determination of the CO_2-brine interfacial tension using graphical alternating conditional expectation. Energy Fuels 28,

624–635.

Mahzari, P., Jones, A.P., Oelkers, E.H., 2019. An integrated evaluation of enhanced oil recovery and geochemical processes for carbonated water injection in carbonate rocks. J. Pet. Sci. Eng. 181.

Messabeb, H., Contamine, F., Cézac, P., Serin, J.P., Pouget, C., Gaucher, E.C., 2017. Experimental Measurement of CO_2 Solubility in Aqueous $CaCl_2$ Solution at Temperature from 323.15 to 423.15 K and Pressure up to 20 MPa Using the Conductometric Titration. J. Chem. Eng. Data 62, 4228–4234.

Nasralla, R.A., Nasr-El-Din, H.A., 2014. Double-layer expansion: Is it a primary mechanism of improved oil recovery by low-salinity waterflooding? SPE Reserv. Eval. Eng. 17, 49–59.

Pereira, L.M.C., Chapoy, A., Burgass, R., Tohidi, B., 2017. Interfacial tension of CO_2 + brine systems: Experiments and predictive modelling. Adv. Water Resour. 103, 64–75.

Pérez-Salado Kamps, Á., Jödecke, M., Xia, J., Vogt, M., Maurer, G., 2006. Influence of salts on the solubility of carbon dioxide in (water + methanol). Part 1: Sodium chloride. Ind. Eng. Chem. Res. 45, 1505–1515.

Rostami, P., Mehraban, M.F., Sharifi, M., Dejam, M., Ayatollahi, S., 2019. Effect of water salinity on oil/brine interfacial behaviour during low salinity waterflooding: A mechanistic study. Petroleum 5, 367–374.

Ruidiaz, E.M., Winter, A., Trevisan, O. V., 2018. Oil recovery and wettability alteration in carbonates due to carbonate water injection. J. Pet. Explor. Prod. Technol. 8, 249–258.

Rumpf, B., Nicolaisen, H., Öcal, C., Maurer, G., 1994. Solubility of carbon dioxide in aqueous

solutions of sodium chloride: Experimental results and correlation. J. Solution Chem. 23, 431–448.

Seyyedi, M., Mahzari, P., Sohrabi, M., 2018. A comparative study of oil compositional variations during CO_2 and carbonated water injection scenarios for EOR. J. Pet. Sci. Eng. 164, 685–695.

Seyyedsar, S.M., Farzaneh, S.A., Sohrabi, M., 2016. Experimental investigation of tertiary CO_2 injection for enhanced heavy oil recovery. J. Nat. Gas Sci. Eng. 34, 1205–1214.

Shaddel, S., Tabatabae-Nejad, S.A., Fathi, S.J., 2014. Low-salinity water flooding: Evaluating the effect of salinity on oil andwater relative permeability, wettability, and oil recovery. Spec. Top. Rev. Porous Media 5, 133–143.

Sharma, M.M., Filoco, P.R., 2000. Effect of brine salinity and crude-oil properties on oil recovery and residual saturations. SPE J. 5, 293–300.

Sharma, T., Iglauer, S., Sangwai, J.S. 2016. Silica Nanofluids in an Oilfield Polymer Polyacrylamide: Interfacial Properties, Wettability Alteration, and Applications for Chemical Enhanced Oil Recovery. Ind. Eng. Chem. Res. 55, 12387–12397.

Sheng, J.J., 2014. Critical review of low-salinity waterflooding. J. Pet. Sci. Eng.

Shojaati, F., Mousavi, S.H., Riazi, M., Torabi, F., Osat, M., 2017. Investigating the Effect of Salinity on the Behavior of Asphaltene Precipitation in the Presence of Emulsified Water. Ind. Eng. Chem. Res. 56, 14362–14368.

Teklu, T.W., Alameri, W., Graves, R.M., Kazemi, H., AlSumaiti, A.M., 2016. Low-salinity water-alternating-CO_2 EOR. J. Pet. Sci. Eng. 142, 101–118.

Weiss, R.F., 1974. Carbon dioxide in water and seawater: the solubility of a non-ideal gas. Mar. Chem. 2, 203–215.

Yang, J., Dong, Z., Dong, M., Yang, Z., Lin, M., Zhang, J., Chen, C., 2016. Wettability Alteration during Low-Salinity Waterflooding and the Relevance of Divalent Ions in This Process. Energy Fuels 30, 72–79.

Yousef, A.A., Al-Saleh, S., Al-Kaabi, A., Al-Jawfi, M., 2011. Laboratory investigation of the impact of injection-water salinity and ionic content on oil recovery from carbonate reservoirs. SPE Reserv. Eval. Eng. 14, 578–593.

Yu, H., Rui, Z., Chen, Z., Lu, X., Yang, Z., Liu, J., Qu, X., Patil, S., Ling, K., Lu, J., 2019. Feasibility study of improved unconventional reservoir performance with carbonated water and surfactant. Energy 182, 135–147.

Zhang, Y., Zhao, B., Jiang, J., Zhuo, Y., Wang, S., 2016. The use of TiO_2 nanoparticles to enhance CO_2 absorption. Int. J. Greenh. Gas Control 50, 49–56.

Zhao, F., Hao, H., Hou, J., Hou, L., Song, Z., 2015. CO_2 mobility control and sweep efficiency improvement using starch gel or ethylenediamine in ultra-low permeability oil layers with different types of heterogeneity. J. Pet. Sci. Eng. 133, 52–65.

Tables

Table 1

Compositional details and physical properties of the crude oil used in this study.

Acid number (mg of KOH/g)	Base number (mg of KOH/g)	Pour point (K)	Viscosity (mPa.s)	Density (gm/cc)	API gravity
1.92	2.82	310	5.1 (323 K)	0.85 (323 K)	37.56 (323 K)
			2.7 (353 K)	0.83 (353 K)	40.01 (353 K)

SARA results (wt%)	Saturate	Asphaltene	Resin	Aromatic
	64.6	18.4	12.9	4.1

Table 2

Petro-physical properties of synthetic sand-pack columns used for flooding experiments.

Sand-pack dimension (cm)	Sand-pack/run no.	Porosity (%)	Average Permeability (md)	Irreducible water saturation (% PV)	Nomenclature	Temperature (K)	Injection Fluid
D = 3.81 and L = 61	1	33.20	782	32.34	run-1	323	Water
	2	31.92	720	33.48	run-2		1 wt% NaCl solution
	3	31.83	690	32.96	run-3		2 wt% NaCl solution
	4	30.84	742	31.98	run-4		3 wt% NaCl solution
	5	29.84	696	31.68	run-5		4 wt% NaCl solution
	6	32.48	810	32.14	run-6	353	Water
	7	32.58	792	31.89	run-7		1 wt% NaCl solution
	8	31.62	788	32.44	run-8		2 wt% NaCl solution
	9	30.22	720	32.56	run-9		3 wt% NaCl solution
	10	29.72	744	32.81	run-10		4 wt% NaCl solution
	11	34.14	784	31.87	run-11	323	Water
	12	32.20	744	32.49	run-12		1 wt% NaCl solution
	13	31.84	738	32.22	run-13		1 wt% NaCl solution
	14	31.96	752	32.18	run-14		1 wt% NaCl solution
	15	32.11	732	32.45	run-15		1 wt% NaCl solution

Figures
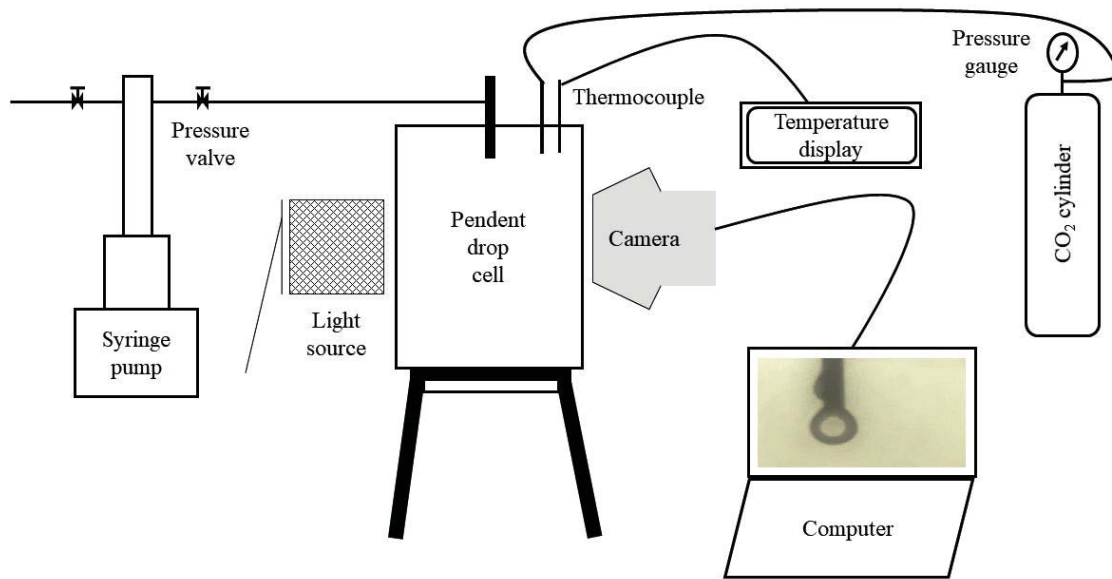
Fig. 1. Schematic of experimental setup used for the pendant drop analysis
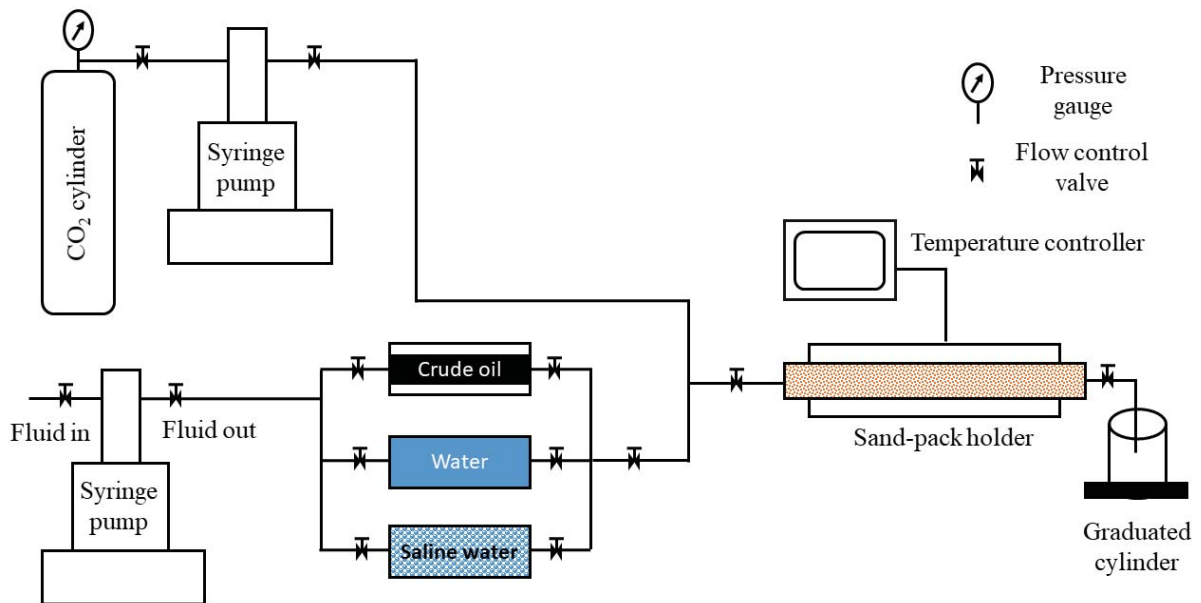
Fig. 2. Schematic of equipment used to perform the oil recovery experiments
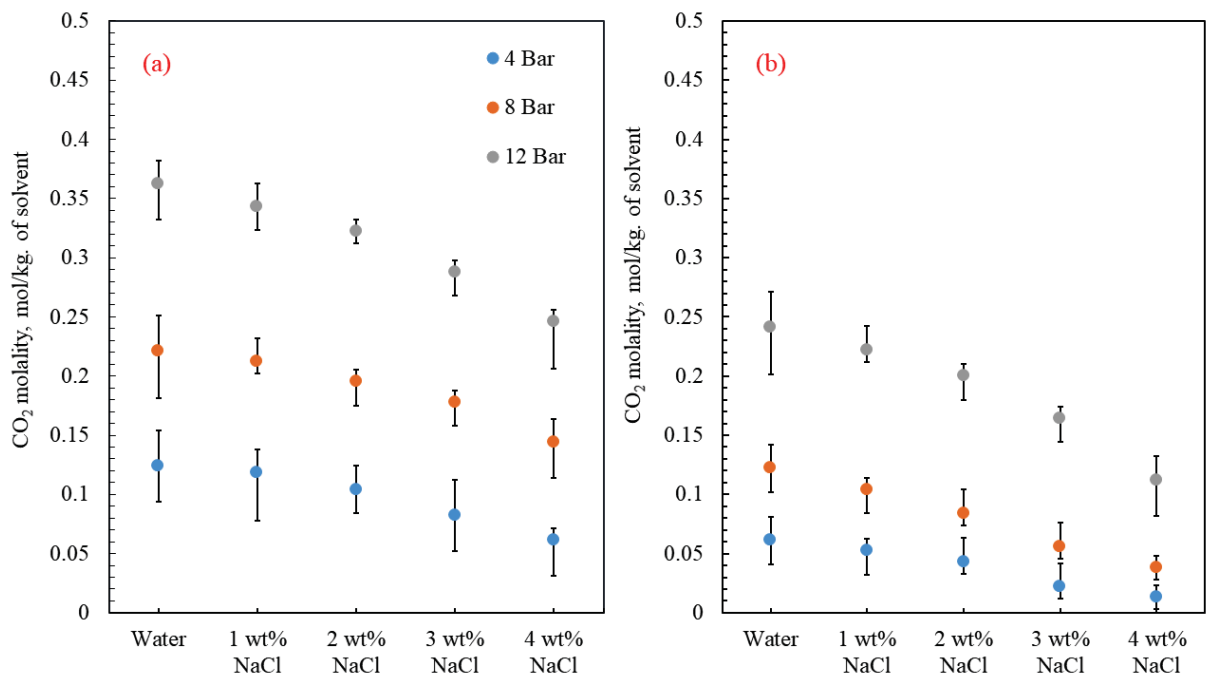
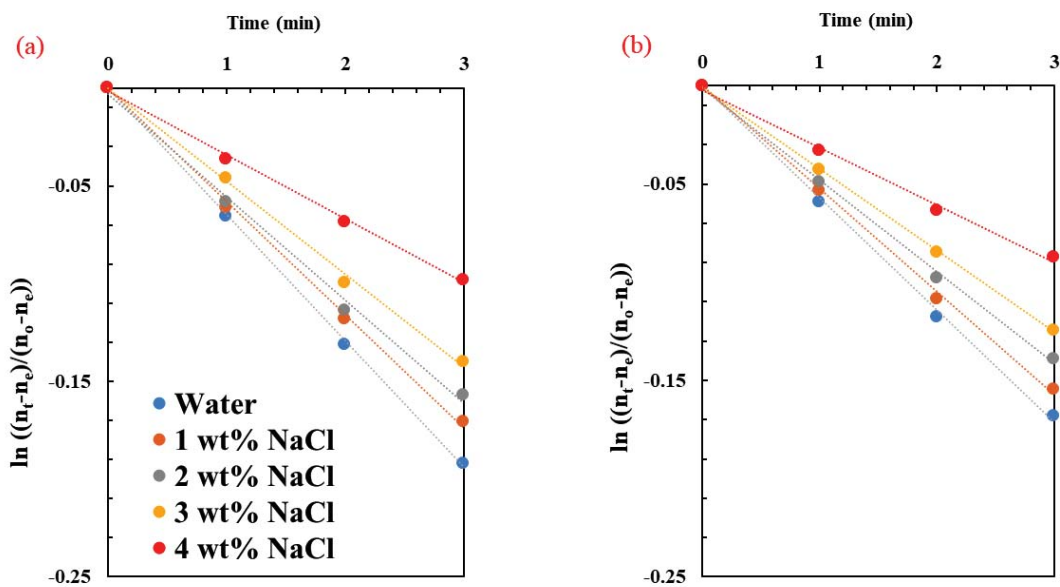**Fig. 3.** CO$_2$ molality results for water solutions of varying salinity (0-4 wt%); (a) 323 K: (b) 353 K.

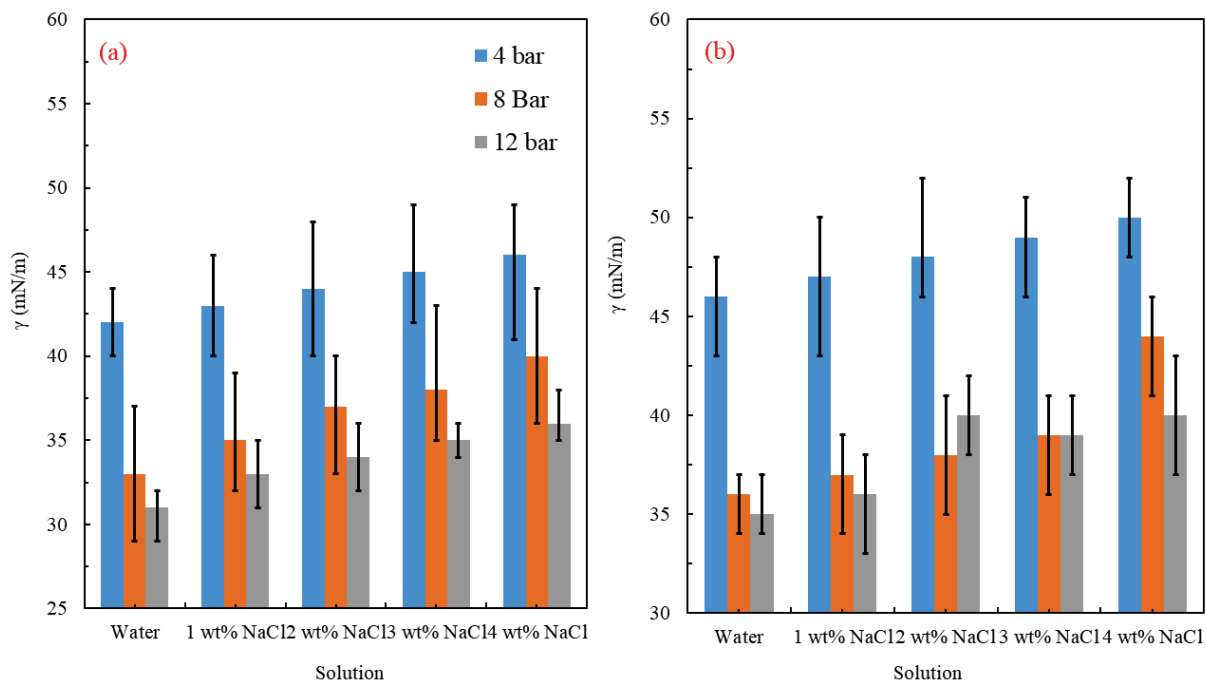**Fig. 4.** CO$_2$ absorption kinetic results for water solutions of varying salinity (0-4 wt%); (a) 323 K: (b) 353 K.

Fig. 5. CO_2- saline water solution interfacial tensions at varying pressure (4-12 bar); (a) 323 K: (b) 353 K.
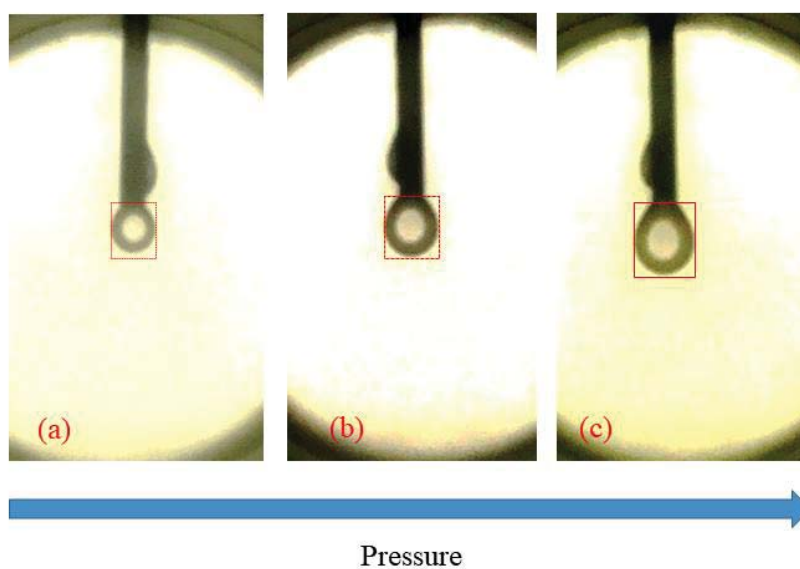
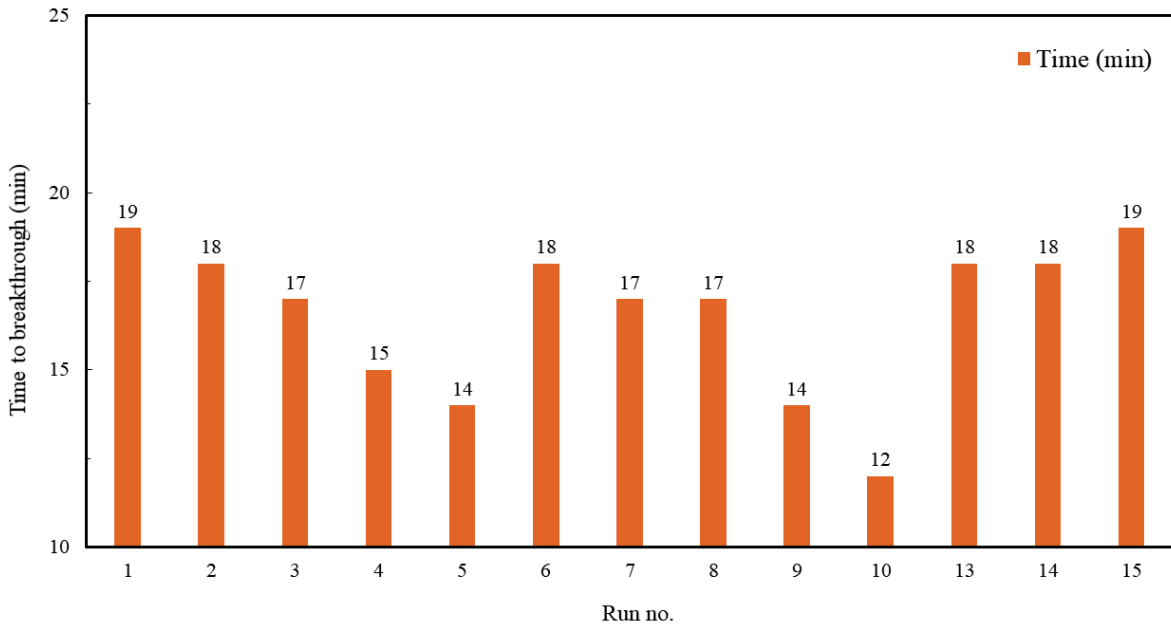**Fig. 6.** Effect of increasing pressure [(a): 4, (b): 8, and (c): 12 bar] on droplet size of 1 wt% NaCl solution inside the pendent drop cell at 323 K.

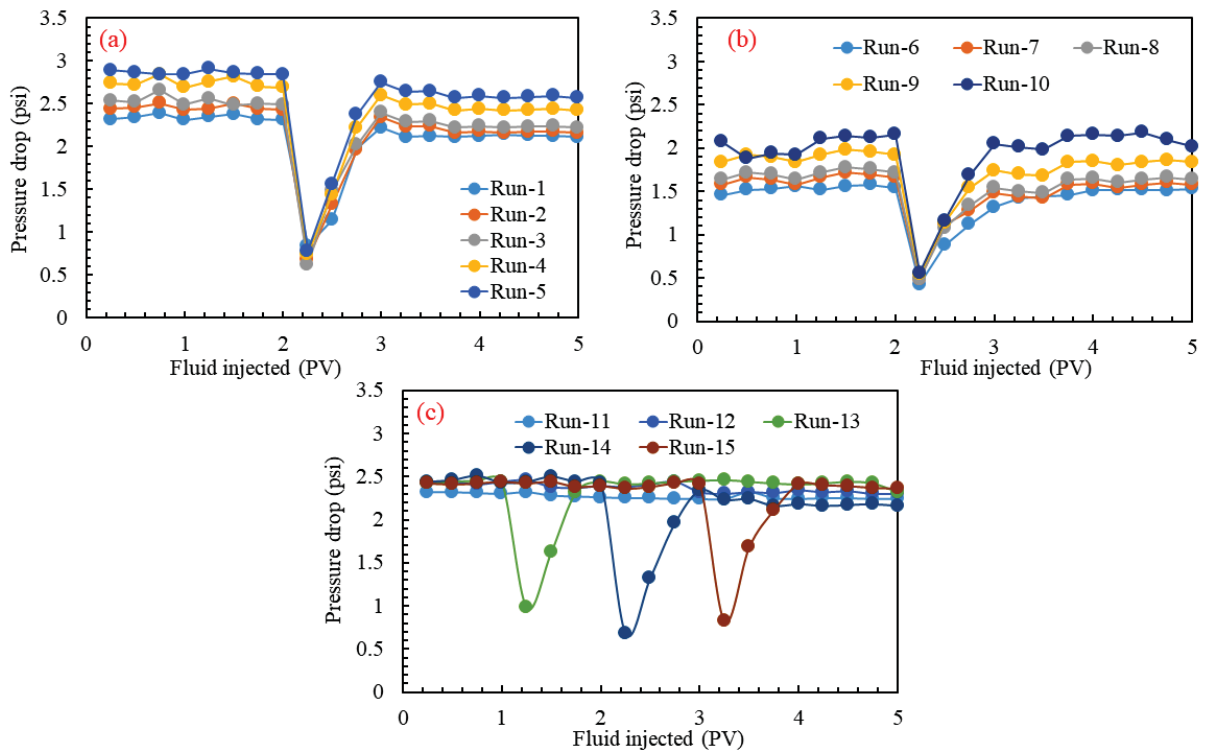**Fig. 7.** Values of time to breakthrough plotted for each of the oil recovery runs.

Fig. 8. Pressure drop as a function of fluid injected (PV) in sand-packs for various runs at temperature (a) 323 K, (b) 353 K, and (c) 323 K with the varying rates of CO_2 injection.
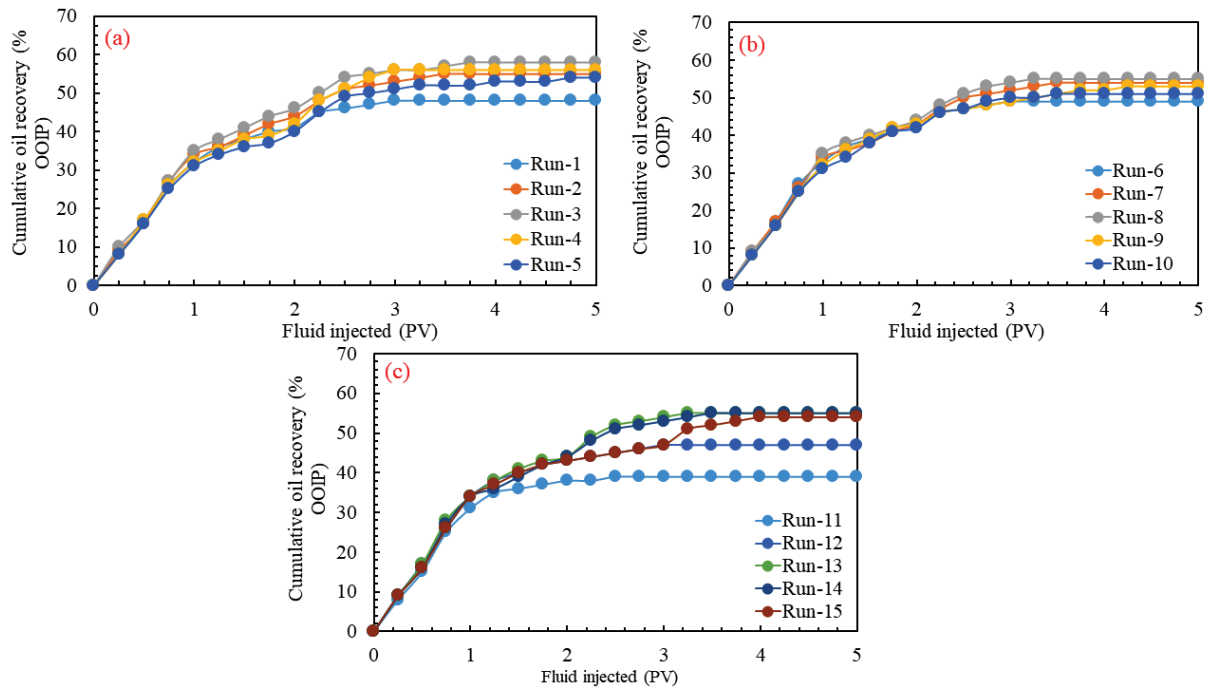
Fig. 9. Resultant oil recovery (%OOIP) as a function of fluid injected (PV) in sand-packs for different flooding experiments at a test temperature of (a) 323 K, (b) 353 K and (c) 323 K with a varying instance of CO_2 injection.
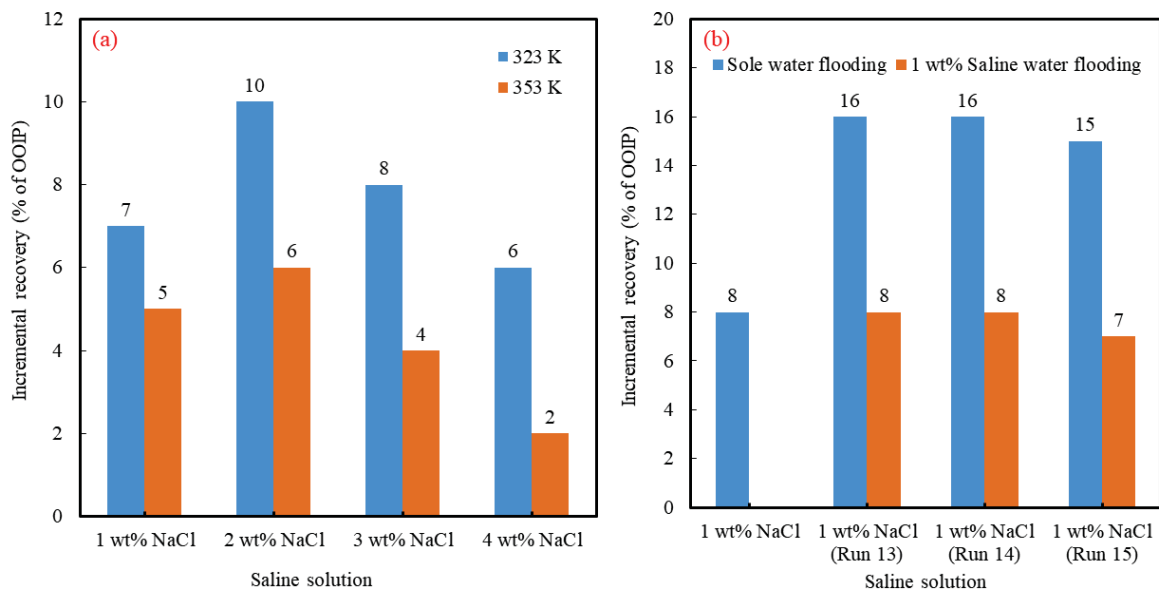

Fig. 10. Plot of comparative oil recovery of various saline solutions at different test temperature.